Schwinger model on an interval: Analytic results and DMRG

Takuya Okuda*

Graduate School of Arts and Sciences, University of Tokyo Komaba, Meguro-ku, Tokyo 153-8902, Japan

(Received 25 October 2022; accepted 2 March 2023; published 17 March 2023)

Quantum electrodynamics in $1+1$ dimensions (Schwinger model) on an interval admits lattice discretization with a finite-dimensional Hilbert space and is often used as a testbed for quantum and tensor network simulations. In this work we clarify the precise mapping between the boundary conditions in the continuum and lattice theories. In particular we show that the conventional Gauss law constraint commonly used in simulations induces a strong boundary effect on the charge density, reflecting the appearance of fractionalized charges. Further, we obtain by bosonization a number of exact analytic results for local observables in the massless Schwinger model. We compare these analytic results with the simulation results obtained by the density matrix renormalization group method and find excellent agreements.

DOI: 10.1103/PhysRevD.107.054506

I. INTRODUCTION

Quantum electrodynamics in $1+1$ dimensions, also known as the Schwinger model [1], is one of the simplest nontrivial gauge theories. Since its introduction in the 1960s it has been widely studied. These days it is often used as a toy model to benchmark numerical techniques for quantum gauge theories, such as tensor network and quantum simulations. See, for example, [2–25].

With the recent rapid development of quantum devices, quantum simulation of gauge theory is becoming more feasible. For this purpose, as in classical simulation, we need to discretize the gauge theory and put it on a finite lattice. In the noisy intermediate-scale quantum (NISQ) era [26], the number of available qubits and the physical volume of the space on which the gauge theory is simulated will be limited. For this reason, simple $(1+1)$-dimensional gauge theories such as the Schwinger model are natural targets of quantum simulation. Putting these theories on a spatial interval rather than a circle has an advantage because the Gauss law constraint allows us to remove gauge fields completely on an interval, while on a circle there remains an infinite-dimensional Hilbert space. The spatial interval for the continuum model corresponds to the open boundary condition of the lattice model. It is thus desirable to know the precise correspondence between the theories in the continuum and on the lattice. To compare the continuum and lattice formulations, it also helps to have analytic results that take into account the strong effects of the boundaries and the finite volume. Rather surprisingly, the study of such effects in the literature is limited.[1]

With these motivations, in this paper we study the Schwinger model on a finite interval and clarify the precise mapping between the continuum (original and bosonized) and lattice models. In particular, we show that the commonly used Gauss law constraint [31] in the lattice formulation induces fractionalized charges on the boundaries, and demonstrate that for an alternative constraint [32] the boundary charges are also modified.[2] Along the way we establish the precise correspondence between the boundary conditions in different formulations. We also derive a number of analytic expressions for physical observables in the ground state in the massless case. This is possible because bosonization maps the massless Schwinger model to a free scalar theory [34,35]. Some of these analytic results were used in [36] to compare with the results of digital quantum simulation of the lattice Schwinger model on a classical simulator.

The paper is organized as follows. In Sec. II we review the continuum Schwinger model in the original formulation. In Sec. II B we study the Schwinger model on an interval using bosonization and derive some analytic results. Section III contains our study of the Kogut-Susskind lattice formulation of the Schwinger model on a finite lattice with the open boundary condition. We review two equivalent formulations, one based on the staggered fermion and another based on spin variables. We compute

*takuya@hep1.c.u-tokyo.ac.jp

[1]See [27,28] for the study of the model on a circle with finite radius, and [29,30] for an earlier study of boundary effects.

[2]If the periodic boundary condition is chosen, then the modification of the Gauss law is equivalent to the mass shift studied in [33] via a field redefinition.

by the density matrix renormalization group (DMRG) [37,38] some physical observables in the ground state and find agreement with the analytic results from Sec. II B, using the original and modified Gauss law constraints. We conclude the paper with discussion in Sec. IV. In Appendix A we calculate the energy in the presence of probe charges using the method of images. In Appendix B we show that the general lattice QCD in the Kogut-Susskind formulation [39] enjoys an exact one-form symmetry for the part of the center of the gauge group under which the matter fermions are neutral.

II. CONTINUUM SCHWINGER MODEL ON AN INTERVAL

In this section we study the continuum Schwinger model on an interval. We first review the original fermionic formulation of the model. Then we review the bosonized version and derive a number of new analytic results for local observables.

A. Review of the fermionic formulation

We use notations $x^0 = t$, $x^1 = x$ for spacetime coordinates and use the Minkowski metric $\eta_{\mu\nu} = \mathrm{diag}(1,-1)$ to raise and lower indices. The dynamical fields in the Schwinger model are the gauge field A_μ ($\mu = 0, 1$) and the Dirac fermion $\psi = (\psi_u, \psi_d)^T$, which is a two-component spinor. Let g be the gauge coupling and m the fermion mass. The model is defined by the action

$$S = \int d^2x \left[-\frac{1}{4} F_{\mu\nu}F^{\mu\nu} + \frac{g\Theta(x)}{4\pi}\epsilon_{\mu\nu}F^{\mu\nu} + \mathrm{i}\bar{\psi}\gamma^\mu(\partial_\mu + \mathrm{i}gA_\mu)\psi - m\bar{\psi}\psi \right] + \text{boundary terms}. \quad (1)$$

We use the notations

$$\epsilon_{01} = -\epsilon^{01} = 1, \quad \gamma^0 = \sigma^3, \quad \gamma^1 = \mathrm{i}\sigma^2, \quad \gamma^5 = \gamma^0\gamma^1, \quad (2)$$

and $\bar{\psi} = \psi^\dagger\gamma^0$. We allow the theta angle to be position dependent and denote it by $\Theta(x)$.

Consider, for example,

$$\Theta_{(q,\theta_0)}(x) = \begin{cases} \theta_0 + 2\pi q & \text{for} \quad \ell_0 < x < \ell_0 + \ell \\ \theta_0 & \text{for} \quad \text{otherwise} \end{cases}. \quad (3)$$

See Fig. 1. The discrete changes in the theta angle $\Theta(x)$ correspond to the presence of probe charges. Indeed we can rewrite the relevant part of the action as

$$\int d^2x \frac{\Theta_{(q,\theta_0)}}{4\pi}\epsilon_{\mu\nu}F^{\mu\nu} = \int d^2x \left[\frac{\theta_0}{4\pi}\epsilon_{\mu\nu}F^{\mu\nu} - q[\delta(x-\ell_0) - \delta(x-\ell_0-\ell)]A_0 \right],$$

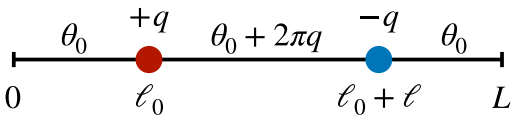

FIG. 1. The setup for $\Theta(x) = \Theta_{(q,\theta_0)}$ in (3), corresponding to probe charges $+q$ at $x = \ell_0$ and $-q$ at $x = \ell_0 + \ell$.

where we explicitly see the pointlike sources for the gauge field.

Let us study the model on an interval $0 \le x \le L$. For the fermion ψ, the general boundary conditions (B.C.s) at each boundary, compatible with the variational principle, are parametrized by a real parameter ν mod $\mathbb{Z}$[3]:

$$\psi_\mathrm{L} + e^{2\pi\mathrm{i}\nu}\psi_\mathrm{R} = 0, \quad (4)$$

where we defined $\psi_\mathrm{L} := (\psi_u + \psi_d)/2$, $\psi_\mathrm{R} := (\psi_u - \psi_d)/2$. We are particularly interested in $(\psi_u, \psi_d, \nu) = (0, \text{arbitrary}, 0), (\text{arbitrary}, 0, \pi)$. Up to a field redefinition $\psi \to \gamma^5\psi$, there are two inequivalent choices [40]: the Ramond (R) B.C.

$$\psi_L(0) = s\psi_R(0) \quad \text{and} \quad \psi_L(L) = s\psi_R(L) \quad (5)$$

and the Neveu-Schwarz (NS) B.C.

$$\psi_L(0) = s\psi_R(0) \quad \text{and} \quad \psi_L(L) = -s\psi_R(L), \quad (6)$$

with $s = \pm 1$.[4]

We work in the temporal gauge $A_0 = 0$, where the Gauss law constraint $\delta S/\delta A_0 = 0$ should be imposed on physical states. Varying A_0, we find the Gauss law

$$\partial_1 F_{01} = \frac{g}{2\pi}\partial_1\Theta + g\bar{\psi}\gamma^0\psi \quad (7)$$

in the bulk. Composite operators such as $\bar{\psi}\gamma^0\psi$ should be defined by some normal ordering [41]. Throughout this paper we make this implicit and omit normal ordering symbols for the fermion. We will specify the B.C.s on F_{01} at $x = 0$ and $x = L$ in Sec. II B where we study the continuum model in the bosonized formulation. The boundary terms in (1), which we do not write explicitly, should be chosen so that they are compatible with the B.C.s.

The canonical momentum conjugate to A^1 ($=-A_1$) is

$$\Pi = \partial_0 A^1 + \frac{g}{2\pi}\Theta. \quad (8)$$

[3]These B.C.s preserve (explicitly break) the vector (axial) $U(1)$ symmetry generated by $\bar{\psi}\gamma^\mu\psi$ ($\bar{\psi}\gamma^\mu\gamma^5\psi$).

[4]Let us extend the domain of $\psi_\mathrm{L}(x)$ to $[-L, L]$ by $\psi_\mathrm{L}(x) := -e^{2\pi\mathrm{i}\nu_0}\psi_\mathrm{R}(-x)$ for $-L \le x \le 0$. Since $\psi_\mathrm{L}(L) = e^{2\pi\mathrm{i}(\nu_1-\nu_0)} \times \psi_\mathrm{L}(-L)$, ψ_L is periodic (antiperiodic) for the R (NS) B.C.

The density $\mathcal{H}$ of the Hamiltonian $H = \int_0^L dx\mathcal{H}(x)$ is

$$\mathcal{H}(x) = \frac{1}{2}\left(\Pi - \frac{g\Theta(x)}{2\pi}\right)^2 - \mathrm{i}\bar{\psi}\gamma^1(\partial_1 + \mathrm{i}gA_1)\psi + m\bar{\psi}\psi.$$

Let us denote the expectation value of the operator $\mathcal{O}$ in the ground state by $\langle\mathcal{O}\rangle$. Local observables of the continuum Schwinger model on an interval include the energy density $\langle\mathcal{H}\rangle$, the charge density $\langle\bar{\psi}\gamma^0\psi\rangle$, the chiral condensate $\langle\bar{\psi}\psi\rangle$, and the electric field F_{01}.

B. Bosonized Schwinger model

In this subsection we study the Schwinger model in the bosonized formulation. There is some overlap with the Appendix of [36] that uses the same convention, and we refer the reader to that paper for details omitted here.

The bosonized Lagrangian density is (cf. [42])

$$\mathcal{L} = -\frac{1}{4}F_{\mu\nu}F^{\mu\nu} + \frac{g}{4\pi}\Theta(x^1)\epsilon^{\mu\nu}F_{\mu\nu} + \frac{g}{\sqrt{\pi}}\epsilon^{\mu\nu}A_\mu\partial_\nu\phi + \frac{1}{2}\partial_\mu\phi\partial^\mu\phi + mg\frac{\mathrm{e}^\gamma}{2\pi^{3/2}}\cos(2\sqrt{\pi}\phi). \tag{9}$$

We choose an appropriate boundary condition on the gauge field so that the solution to the Gauss law constraint is

$$F_{01} - \frac{g}{2\pi}\Theta = \frac{g}{\sqrt{\pi}}\phi. \tag{10}$$

The Hamiltonian density is given as

$$\mathcal{H} \coloneqq \frac{1}{2}(\Pi_\phi)^2 + \frac{1}{2}(\partial_x\phi)^2 + \frac{\mu^2}{2}\left(\phi + \frac{\Theta(x)}{2\sqrt{\pi}}\right)^2 - mg\frac{\mathrm{e}^\gamma}{2\pi^{3/2}}:\cos(2\sqrt{\pi}\phi):_\infty, \tag{11}$$

where Π_ϕ is the canonical momentum conjugate to ϕ and $\mu \equiv g/\sqrt{\pi}$. We write $:\bullet:_\infty$ for the normal ordering (see below) with respect to the creation-annihilation operators defined in the infinite volume and used the relation

$$\bar{\psi}\psi = -\frac{\mathrm{e}^\gamma}{2\pi^{3/2}}g:\cos[2\sqrt{\pi}\phi(x)]:_\infty, \tag{12}$$

where $\gamma \simeq 0.58$ is the Euler constant. The particular numerical coefficient $\mathrm{e}^\gamma/(2\pi^{3/2})$ is correct for this choice of normal ordering.[5]

We study the bosonized model with $m = 0$ and the Dirichlet boundary conditions

$$\phi = \sqrt{\pi}w_0 \quad \text{at } x = 0, \qquad \phi = \sqrt{\pi}w_1 \quad \text{at } x = L. \tag{13}$$

[5]See [43] for a general discussion of normal ordering.

We set $k_n \coloneqq \pi n/L$. Let us define

$$\phi_0(x) \coloneqq \sqrt{\pi}w_0 + \sqrt{\pi}(w_1 - w_0)\frac{x}{L}, \tag{14}$$

$$\hat{\phi}(x) \coloneqq \phi(x) - \phi_0(x), \qquad \hat{\Theta}(x) \coloneqq \Theta(x) + 2\sqrt{\pi}\phi_0(x). \tag{15}$$

Let us consider the Fourier expansions

$$\Pi_\phi(x) = \sum_{n=1}^\infty \Pi_n \sin(k_n x), \qquad \hat{\phi}(x) = \sum_{n=1}^\infty \phi_n \sin(k_n x),$$
$$\hat{\Theta}(x) = \sum_{n=1}^\infty \Theta_n \sin(k_n x).$$

The Hamiltonian becomes

$$H_{\text{boson}} = \frac{\pi(w_1 - w_0)^2}{2L} + \sum_{n=1}^\infty\left[\omega_n\left(a_n^\dagger a_n + \frac{1}{2}\right) + \frac{L\mu^2}{16}\frac{k_n^2}{\omega_n^2}\Theta_n^2\right], \tag{16}$$

where $\omega_n = \sqrt{\mu^2 + k_n^2}$ and

$$a_n = \frac{\sqrt{L\omega_n}}{2}\left(\phi_n + \frac{\mu^2\Theta_n}{2\sqrt{\pi}\omega_n^2}\right) + \frac{\mathrm{i}}{2}\sqrt{\frac{L}{\omega_n}}\Pi_n. \tag{17}$$

We have $[a_n, a_{n'}^\dagger] = \delta_{nn'}$. The ground state $|0\rangle$ satisfies $a_n|0\rangle = 0$ and has a divergent energy due to the terms proportional to ω_n, which are independent of Θ.

The energy density $\langle 0|\mathcal{H}(x)|0\rangle$ is also UV divergent. Let $\lfloor x\rfloor$ denote the largest integer smaller than or equal to x. With a cutoff $k_n \le \Lambda$,[6] the regularized energy density is

$$\mathcal{E}_\Lambda(x) = \frac{1}{2L}\sum_{n=1}^{\lfloor L\Lambda/\pi\rfloor}\left[\left(\omega_n + \frac{\mu^2}{\omega_n}\right)\sin^2(k_n x) + \frac{k_n^2}{\omega_n}\cos^2(k_n x)\right] + \frac{1}{8\pi}\left[\left(\sum_{n=1}^{\lfloor L\Lambda/\pi\rfloor}\frac{\mu^2 k_n}{\omega_n^2}\Theta_n\cos(k_n x)\right)^2 + \left(\sum_{n=1}^{\lfloor L\Lambda/\pi\rfloor}\frac{\mu k_n^2}{\omega_n^2}\Theta_n\sin(k_n x)\right)^2\right], \tag{18}$$

which is quadratically divergent. On a full infinite line without probe charges, the corresponding regularized energy density is, with $\omega(k) \coloneqq \sqrt{k^2 + \mu^2}$,[7]

[6]For plots throughout the paper, we use *Mathematica* to evaluate regularized sums numerically by setting $\lfloor L\Lambda/\pi\rfloor$ to 10^4.

[7]Explicitly, $\mathcal{E}_\Lambda^{\text{line}} = [(\Lambda^2 + \mu^2)^{1/2}\Lambda + \mu^2\sinh^{-1}(\Lambda/\mu)]/4\pi$.

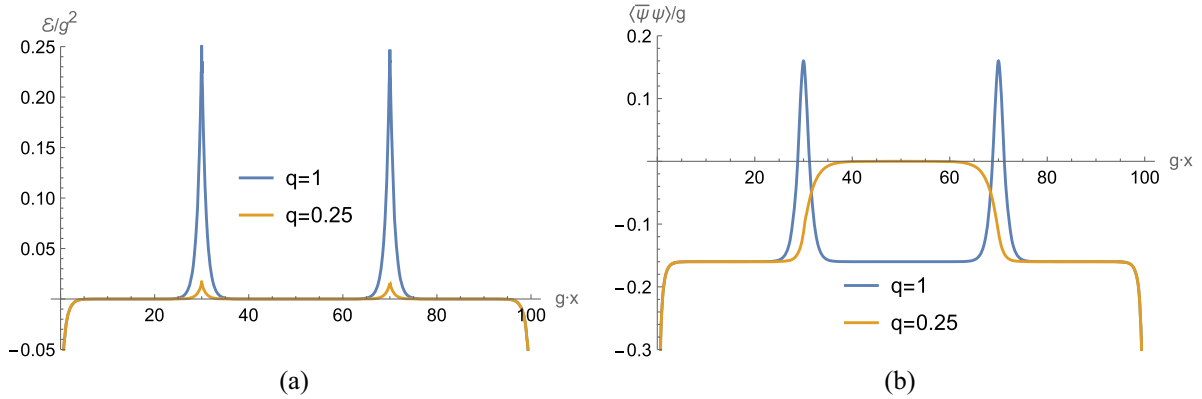

FIG. 2. (a) Renormalized energy density $\mathcal{E}$ given by (20), for two probe charges $\pm q$ placed at $x = (L \mp \ell)/2$ represented by the position-dependent theta angle (26), for $L = 100\ \mathrm{g}^{-1}$ and $\ell = 40\ \mathrm{g}^{-1}$. The local behaviors near each boundary and each pole are given by (31) and (36), respectively. (b) Chiral condensate $\langle\bar\psi\psi(x)\rangle$ given by (21) for the same setup. The local behaviors near each boundary and each pole are given by (34) and (37), respectively.

$$\mathcal{E}_\Lambda^{\mathrm{line}} \coloneqq \lim_{L\to\infty} \mathcal{E}_\Lambda(L/2) = \int_0^\Lambda \frac{dk}{2\pi}\omega(k). \tag{19}$$

We define the renormalized energy density as

$$\mathcal{E}(x) \coloneqq \lim_{\Lambda\to\infty} (\mathcal{E}_\Lambda(x) - \mathcal{E}_\Lambda^{\mathrm{line}}). \tag{20}$$

An expression for the chiral condensate was found in [36]:

$$\langle\bar\psi\psi(x)\rangle = -\frac{e^\gamma g}{2\pi^{3/2}}\lambda(x) \times \cos\left[2\sqrt{\pi}\phi_0(x) - \sum_{n=1}^\infty \frac{\mu^2}{\omega_n^2}\Theta_n \sin(k_n x)\right], \tag{21}$$

where[8]

$$\lambda(x) \coloneqq \lim_{\Lambda\to\infty} \exp\left[\sinh^{-1}\left(\frac{\Lambda}{\mu}\right) - \sum_{n=1}^{\lfloor L\Lambda/\pi\rfloor} \frac{2\pi}{L}\frac{\sin^2(k_n x)}{\sqrt{\mu^2+k_n^2}}\right]. \tag{23}$$

For the charge density $\bar\psi\gamma^0\psi(x) = \partial_x\phi/\sqrt{\pi}$, we obtain

$$\langle\bar\psi\gamma^0\psi(x)\rangle = \frac{w_1 - w_0}{L} - \frac{\mu^2}{2\pi}\sum_{n=1}^\infty \frac{k_n}{\omega_n^2}\Theta_n \cos(k_n x). \tag{24}$$

For the electric field we have

$$\langle F_{01}\rangle = \frac{g}{2\pi}\sum_{n=1}^\infty \frac{k_n^2}{\omega_n^2}\Theta_n \sin(k_n x). \tag{25}$$

Below, we consider special and limiting cases.

1. Two probe charges on an interval

For probe charges on an interval, one can evaluate the sums above. As an example, let us consider

$$\Theta_{\mathrm{pair}}(x) = \begin{cases} 2\pi q & \text{for } \frac{L-\ell}{2} \le x \le \frac{L+\ell}{2} \\ 0 & \text{otherwise} \end{cases}, \tag{26}$$

which represent a pair of charges $\pm q$ placed at $x = (L \mp \ell)/2$, i.e., $\Theta_{\mathrm{pair}} = \Theta_{q,\theta_0=0}|_{\ell_0=(L-\ell)/2}$. We impose the boundary conditions $\phi = 0$ at $x = 0, L$ corresponding to $w_0 = w_1 = 0$. The nonzero Fourier coefficients are

$$(\Theta_{\mathrm{pair}})_{2j+1} = \frac{8q}{2j+1}(-1)^j \sin\left[k_{2j+1}(\ell/2)\right] \tag{27}$$

for $j \in \mathbb{Z}_{>0}$. The total energy E_{pair}, defined as the energy computed from (16) by removing terms proportional to ω_n, was obtained in [36][9]:

$$E_{\mathrm{pair}} = \frac{\sqrt{\pi}}{2}q^2 g\frac{(1-e^{-\mu\ell})(1+e^{-\mu(L-\ell)})}{1+e^{-\mu L}}. \tag{28}$$

The energy density $\mathcal{E}(x)$ in (20) computed for (26) is plotted in Fig. 2(a).[10] The chiral condensate $\langle\bar\psi\psi(x)\rangle$ in (21) corresponding to (26) is plotted in Fig. 2(b). For the cosine in (21), the residue method gives its argument explicitly as

[8]By several manipulations, one may rewrite (23) as

$$\log\lambda(x) = \int_1^\infty \frac{du}{\sqrt{u^2-1}}\left(\frac{-2}{e^{2\mu L u}-1} + \frac{\cosh\left[(2x/L-1)\mu L u\right]}{\sinh[\mu L u]}\right). \tag{22}$$

[9]In Appendix A, we give an alternative derivation of (28) by the method of images.

[10]It is possible to perform the summations in (18) to obtain an alternative expression. We found the result to be not illuminating.

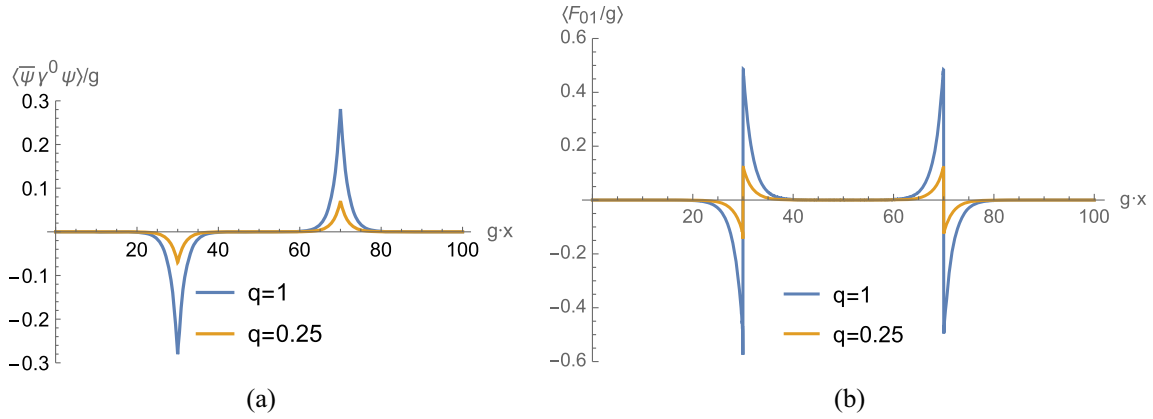

(a) (b)

FIG. 3. (a) Charge density $\langle\bar{\psi}\gamma^0\psi(x)\rangle$ given by (24) or equivalently by (29) for the same setup as for Fig. 2. The local behaviors near the probes are given by (38). (b) Electric field F_{01} given by (25) or equivalently by (30) for the same setup.

$$-\pi q\sum_{j=0,1}(-1)^{\lfloor\eta_j(x)\rfloor}\left(\frac{\cosh[(\{\eta_+(x)\}-1/2)\mu L]}{\cosh(\mu L/2)}-1\right),$$

where $\eta_0(x) \coloneqq (x-\frac{L-\ell}{2})/L$, $\eta_1(x) \coloneqq (x-\frac{L+\ell}{2})/L$, and $\{\eta\} \coloneqq \eta - \lfloor\eta\rfloor$. The charge density $\langle\bar{\psi}\gamma^0\psi(x)\rangle$ that corresponds to (26) is plotted in Fig. 3(a). The summation in (24) can be performed explicitly to give

$$\langle\bar{\psi}\gamma^0\psi(x)\rangle_{\text{pair}} = \frac{q\mu}{2\cosh(\mu L/2)}\sum_{j=0,1}(-1)^{j+\lfloor\eta_j(x)\rfloor} \times \sinh\left[(\{\eta_j(x)\}-1/2)\mu L\right]. \tag{29}$$

The electric field that corresponds to (26) is plotted in Fig. 3(b). Performing the summation in (25), we obtain the explicit expression

$$\langle F_{01}\rangle_{\text{pair}} = \frac{qg}{2\cosh(\mu L/2)}\sum_{j=0,1}(-1)^{j+\lfloor\eta_j(x)\rfloor} \times \cosh\left[(\{\eta_j(x)\}-1/2)\mu L\right]. \tag{30}$$

2. Behaviors near a boundary

We now consider the massless Schwinger model on a half-line $[0,\infty)$ with $\Theta(x)=0$ and the boundary condition $\phi(x=0)=0$. Let us begin with the energy density. The regularized energy density on a half-line is obtained from (18) by sending L to infinity: $\mathcal{E}_\Lambda^{\text{half-line}}(x) \coloneqq \lim_{L\to\infty}\mathcal{E}_\Lambda(x)$ We define the renormalized energy density on a half-line as $\mathcal{E}_{\text{half-line}} \coloneqq \lim_{\Lambda\to\infty}(\mathcal{E}_\Lambda^{\text{half-line}}(x)-\mathcal{E}_\Lambda^{\text{line}})$. We find

$$\mathcal{E}_{\text{half-line}} = -\frac{\mu^2}{2\pi}K_0(2\mu x). \tag{31}$$

The modified Bessel function $K_0(z)$ has the asymptotics

$$K_0(z) = \begin{cases} -\log(z/2)-\gamma+\mathcal{O}(z) & \text{for } z\sim 0 \\ \sqrt{\frac{\pi}{2z}}e^{-z}(1+\mathcal{O}(1/z)) & \text{for } z\gg 1 \end{cases}. \tag{32}$$

Thus the energy density diverges logarithmically near the boundary and decays exponentially away from it. From

$$\lim_{L\to\infty}\lambda(x) = \exp\left[\int_0^\infty dk\,\frac{\cos(2kx)}{\sqrt{\mu^2+k^2}}\right] = e^{K_0(2\mu x)}. \tag{33}$$

we get for the chiral condensate

$$\langle\bar{\psi}\psi(x)\rangle_{\text{half-line}} = -\frac{e^\gamma}{2\pi^{3/2}}\,g e^{K_0(2\mu x)}, \tag{34}$$

which is the result obtained in [30]. The condensate diverges as $\langle\bar{\psi}\psi(x)\rangle = \mathcal{O}(x^{-1/2})$ near the boundary and decays exponentially away from it. The charge density and the electric field simply vanish a half-line for $\Theta(x)=0$ and the boundary condition $\phi(x=0)=0$.

3. Behaviors near a probe charge

Let us consider the system with a single probe charge q at $x=x_0$ on an infinite line, which is represented by the position-dependent theta angle

$$\Theta_{\text{probe}}(x) \coloneqq \begin{cases} 0 & \text{for } x<x_0 \\ 2\pi q & \text{for } x>x_0 \end{cases}. \tag{35}$$

By taking an appropriate limit of (18) or by repeating the steps leading to (18), we obtain the energy density (renormalized by subtracting the value without a probe)

$$\mathcal{E}_{\text{probe}}(x) = \frac{\pi}{4}q^2\mu^2 e^{-2\mu|x-x_0|}. \tag{36}$$

In a similar manner one can obtain expressions for other local observables. We obtain, as in Appendix D of [36],

$$\langle\bar{\psi}\psi(x)\rangle_{\text{probe}} = -\frac{e^\gamma g}{2\pi^{3/2}}\begin{cases} \cos\left[\pi q e^{-\mu(x_0-x)}\right] & \text{for } x<x_0 \\ \cos\left[2\pi q-\pi q e^{-\mu(x-x_0)}\right] & \text{for } x>x_0 \end{cases}. \tag{37}$$

We also have

$$\langle\bar{\psi}\gamma^0\psi(x)\rangle_{\text{probe}} = -\frac{q}{2}\mu e^{-\mu|x-x_0|}, \tag{38}$$

which previously appeared in (4.12) of [27]. Integrating this, one obtains

$$\langle F_{01}\rangle_{\text{probe}} = \frac{q}{2} g\,\text{sgn}(x-x_0)e^{-\mu|x-x_0|}. \tag{39}$$

4. Behaviors near a boundary charge

We now consider the massless Schwinger model on a half-line $[0,\infty)$ with $\Theta(x)=0$ and the boundary condition

$$\phi(x=0) = \sqrt{2}w_0 =: q/2 \tag{40}$$

(or equivalently $\Theta(x)=\sqrt{\pi}q$ and $\phi(0)=0$). This can be obtained by setting $w_0 = q/2$ and taking the limit $L\to\infty$. We find that the energy density is the sum of (31) and (36) while the charge density and the electric field are respectively given by (38) and (39) (all with $x_0=0$). The chiral condensate is given by

$$\langle\bar{\psi}\psi(x)\rangle_{\text{boundary char}} = -\frac{e^{\gamma}g}{2\pi^{3/2}} e^{K_0(2\mu x)}\cos(\pi q e^{-\mu x}). \tag{41}$$

III. LATTICE SCHWINGER MODEL WITH OPEN BOUNDARY CONDITIONS

A. Fermion versus spin models on a lattice

Let us turn to the Kogut-Susskind lattice formulation of the Schwinger model [39,44] with a position-dependent theta angle. We will be brief and follow the conventions of [36].

We consider a one-dimensional spatial lattice with N sites, labeled by integers $n=0,1,\ldots,N-1$.[11] The two components $\psi_u(x)$ and $\psi_d(x)$ of the Dirac fermion $\psi=(\psi_u,\psi_d)^T$ are replaced by the staggered fermion χ_n at the even and odd sites with $x=na$, respectively, according to the correspondence

$$\begin{matrix}\psi_u(x)\\ \psi_d(x)\end{matrix} \leftrightarrow \frac{\chi_n}{\sqrt{2a}} \begin{matrix} n\text{: even}\\ n\text{: odd}\end{matrix}. \tag{42}$$

On the nth link, which connects the sites n and $n+1$, we introduce the link variables U_n and L_n satisfying $U_n^\dagger = U_n^{-1}$, $L_n^\dagger = L_n$ according to the correspondence

$$e^{-iagA^1(x)} \leftrightarrow U_n, \qquad -\Pi(x)/g \leftrightarrow L_n. \tag{43}$$

These operators satisfy canonical (anti)commutation relations, among which the nontrivial ones are

$$\{\chi_m,\chi_n^\dagger\} = \delta_{mn}, \qquad [U_m,L_n] = \delta_{mn}U_m. \tag{44}$$

We also introduce the lattice version ϑ_n of the position-dependent theta angle on the nth link:

$$\Theta(x) \leftrightarrow \vartheta_n. \tag{45}$$

The Hamiltonian of the lattice theory is

$$\begin{aligned} H_{\text{lattice}} = {}& \frac{g^2a}{2}\sum_{n=0}^{N-2}\left(L_n+\frac{\vartheta_n}{2\pi}\right)^2 \\ & -\frac{i}{2a}\sum_{n=0}^{N-2}\left(\chi_n^\dagger U_n\chi_{n+1} - \chi_{n+1}^\dagger U_n^\dagger\chi_n\right) \\ & + m\sum_{n=0}^{N-1}(-1)^n\chi_n^\dagger\chi_n, \end{aligned} \tag{46}$$

which is the direct counterpart of (9).

There is a relation between N and the fermion boundary conditions. As in (42) we identify ψ_u (ψ_d) with χ_{even} (χ_{odd}). Since n in χ_n runs from 0 to $N-1$, we effectively have $\chi_{-1}=\chi_N=0$. Thus we have $\psi_d=0$ on the left and $\psi_u=0$ ($\psi_d=0$) on the right for N even (odd), namely there is a correspondence, leading to the NS (R) boundary condition.[12]

As in the continuum theory, the physical Hilbert space is obtained by the Gauss law constraint. The standard choice [31] of the Gauss law constraint is[13]

$$G_n^{\text{standard}} := L_n - L_{n-1} - \chi_n^\dagger\chi_n + \frac{1-(-1)^n}{2} = 0. \tag{47}$$

We impose the boundary condition $L_{-1}=0$ and fix the gauge $U_n=1$ to eliminate (L_n,U_n). The term $(-1)^n/2$ in (47) represents a site-dependent background charge. In the bulk, the spatially averaged background charge density vanishes in the continuum limit, but we will see that there remains a nontrivial localized charge on a boundary and induces a background electric field.

We convert the fermions into spin variables by the Jordan-Wigner transformation [45]

$$\chi_n = \frac{X_n - iY_n}{2}\prod_{i=0}^{n-1}(-iZ_i), \tag{48}$$

where X_n, Y_n, Z_n, respectively, denote the Pauli matrices σ_x, σ_y, σ_z associated with the nth site. Besides the theta

[11] We will see that the behavior of the model depends strongly on whether N is even or odd.

[12] We also checked that the DMRG computation of the spectra of the XY model, which is equivalent to the free fermion model via the Jordan-Wigner transformation for open B.C.s, reproduces the expected spectra of the continuum Dirac fermion obeying the NS (R) boundary conditions for large N even (odd).

[13] Here, the presence of external charges is accounted for, as in (3), by the position-dependent theta angle ϑ_n in (46), cf. (B4).

angle, g and m as in Sec. II, the lattice introduces the lattice spacing a as an extra parameter. The length L of the spatial interval is given by $L = (N-1)a$. The Gauss law constraint reads

$$0 = L_n - L_{n-1} - \frac{Z_n + (-1)^n}{2}. \tag{49}$$

We solve this with the boundary condition

$$L_{-1} = 0. \tag{50}$$

The Hamiltonian in terms of the spin variables is

$$H_{\text{spin}} = \frac{g^2 a}{2}\sum_{n=0}^{N-2}\left[\sum_{i=0}^{n}\frac{Z_i + (-1)^i}{2} + \frac{\vartheta_n}{2\pi}\right]^2 + \frac{1}{4a}\sum_{n=0}^{N-2}(X_n X_{n+1} + Y_n Y_{n+1}) + \frac{m}{2}\sum_{n=0}^{N-1}(-1)^n Z_n. \tag{51}$$

Note the structural similarity between (11) and (51).

We have the following correspondence for the local observables of the continuum theory and the spin model.

$$\mathcal{H}(x)|_{m=0} \leftrightarrow \frac{g^2}{2}\left[\sum_{i=0}^{n}\frac{Z_i + (-1)^i}{2} + \frac{\vartheta_n}{2\pi}\right]^2 + \frac{1}{4a^2}(X_n X_{n+1} + Y_n Y_{n+1}), \tag{52}$$

$$\bar{\psi}\gamma^0\psi(x) \leftrightarrow \frac{1}{4a}(Z_n + Z_{n+1}), \tag{53}$$

$$\bar{\psi}\psi(x) \leftrightarrow \frac{(-1)^n}{4a}(Z_n - Z_{n+1}), \tag{54}$$

$$F_{01} \leftrightarrow g\sum_{i=0}^{n}\frac{Z_i + (-1)^i}{2} + \frac{\vartheta_n}{2\pi}. \tag{55}$$

The quantities on the left- and right-hand sides are for a continuous theory and a lattice model, respectively, requiring renormalization (normal ordering) in the former.

We will often consider the particular form of the position-dependent theta angle corresponding to probe charges $\pm q$ located at the sites $n = \hat{\ell}_0$ $n = (\hat{\ell}_0 + \hat{\ell})$:

$$(\vartheta_{\text{pair}})_n := \begin{cases} 2\pi q + \theta_0, & \hat{\ell}_0 \le n < \hat{\ell}_0 + \hat{\ell} \\ \theta_0, & \text{otherwise} \end{cases}. \tag{56}$$

B. Spin lattice versus bosonized continuum models

Let us compare the Gauss law constraints (10) and (49) in the spin and bosonized formulations, respectively. The correspondence

$$\frac{1}{g}F_{01} - \frac{1}{2\pi}\Theta(x) \leftrightarrow L_n \tag{57}$$

in (43) suggests the correspondence

$$\phi(x) \leftrightarrow \frac{\sqrt{\pi}}{2}\sum_{i=0}^{n}(Z_i + (-1)^i) =: \phi_n. \tag{58}$$

The operator ϕ_n rotates the $X_j Y_j$ planes for $j \le n$. The comparison of (11) and (51) suggests the correspondence

$$\frac{1}{2}(\Pi_\phi)^2 + \frac{1}{2}(\partial_x\phi)^2 + \text{const} \leftrightarrow \frac{1}{4a^2}(X_n X_{n+1} + Y_n Y_{n+1}) =: h_n. \tag{59}$$

Taking the commutators of the both sides of (58) and (59) gives another correspondence

$$\Pi_\phi \leftrightarrow \frac{\sqrt{\pi}}{4a}(Y_n X_{n+1} - X_n Y_{n+1}) =: \pi_n, \tag{60}$$

where the expression on the right arises from $[\phi_m, h_n] = (\mathrm{i}/a)\delta_{mn}\pi_n$. We note the commutation relation

$$[\phi_m, \pi_n] = -\pi\mathrm{i}\delta_{mn}h_n. \tag{61}$$

This reduces to the canonical commutation relation between $\phi(x)$ and $\Pi_\phi(x)$ in the continuum limit because the density of the kinetic term diverges as $-1/(\pi a^2)$[14] so that we can replace h_n by $-1/(\pi a)$ in (61).

The lattice Schwinger model described in Sec. III A should correspond, in the continuum limit, to specific values of w_0 and w_1 in (13). In the Appendix of [36], it was argued that

$$w_0 = \frac{1}{4}, \qquad w_1 = \frac{Q}{2} + \frac{1}{4}, \qquad Q := \sum_{n=0}^{N-1} Z_n. \tag{62}$$

The charge Q is conserved and can be treated as a c number within a fixed charge sector. In fact, if the value of ν in (4) is ν_0 (ν_1) at $x = 0$ ($x = L$), then we have[15]

$$\nu_1 - \nu_0 = w_1 - w_0 \mod \mathbb{Z}. \tag{63}$$

The relations (62) and (63) are nontrivially consistent with the correspondence between with parity of N and the fermion boundary conditions found in Sec. III A. We will

[14]The divergence can be computed by the free fermion because it is not affected by g or m, which only appears as ga or ma.

[15]This should follow from the bosonization rules $\psi_{\mathrm{L(R)}} \sim e^{\mathrm{i}\phi_{\mathrm{L(R)}}}$, where $\phi_{\mathrm{L(R)}}$ is the normalized left-(right-)moving part of ϕ. We checked it by comparing the explicit cylinder partition functions.

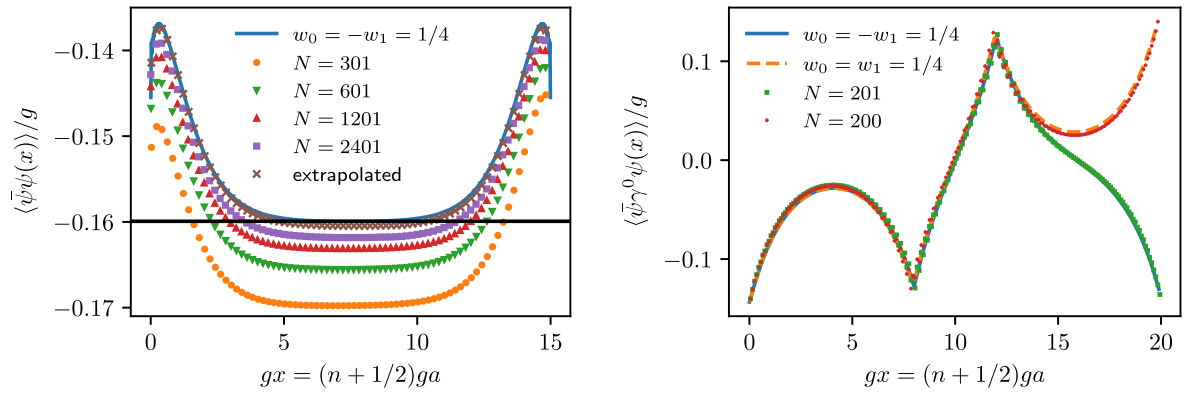

FIG. 4. (a) Chiral condensate for $L = (N-1)a = 15\ g^{-1}$ and $q = 0$ (no probe charge), $m = 0$, and $\theta_0 = 0$. Plots of $(4ga)^{-1}(-1)^n\langle Z_n - Z_{n+1}\rangle$ computed by DMRG and $\langle\bar\psi\psi(x)\rangle/g$ computed analytically by the formula (21) are shown. We also plot the results of extrapolation to $N = \infty$ ($a = 0$) obtained by fitting the data for $N \in \{301, 601, 1201, 2401\}$ by a quadratic function of $1/N$. For better visibility, only a subset of the values of n is used. (b) Charge density for a pair of charges with $g\ell = 4$, $q = 0.5$, and $\theta_0 = m = 0$. Plots of $(4ga)^{-1}\langle(Z_n + Z_{n+1})\rangle$ computed by DMRG and $\langle\bar\psi\gamma^0(x)\rangle/g$ computed analytically by (24) and (26) are shown. The precise length of the interval is $L = (N-1)a$ with $ga = 0.1$.

also explicitly confirm the identification (62) by comparing the charge densities computed by DMRG and by bosonization. We note that the eigenvalue of Q is even (odd) if N is even (odd). Thus the winding number $w_1 - w_0$ is an integer (a half-integer) if N is even (odd). To summarize, we have the correspondence[16]

$$N \text{ even} \leftrightarrow \text{integer winding} \leftrightarrow \text{NS B.C.},$$
$$N \text{ odd} \leftrightarrow \text{half-integer winding} \leftrightarrow \text{R B.C.} \quad (64)$$

C. Comparison of DMRG and analytic results

Here we compare the DMRG results based on the spin formulation in Sec. III and the analytic results based on bosonization in Sec. II B. For our implementation of DMRG, we used the ITensor library [47]. See [48] for a related study.

For the chiral condensate $\propto \langle(-1)^n Z_n\rangle$, we plot the DMRG results including the extrapolated values and the analytical results in Fig. 4(b) for the case with no probe charges. After extrapolation, the DMRG and analytical results match well.

For the charge density, we plot the DMRG and analytic results in Fig. 4(a). We see that they agree very well. This gives strong evidence for the identification (62). Near the right boundary, the charge density profile is identical to that near a probe of charge $-1/2$ for N even and $+1/2$ for N odd. We note that the parameters w_0 and w_1 parametrizing the Dirichlet boundary conditions for ϕ in (13) are related to the boundary charges q_L and q_R on the left and right boundaries as

$$w_0 = \frac{q_L}{2}, \qquad w_1 = -\frac{q_R}{2}, \quad (65)$$

generalizing (40). Therefore, the charges on the boundaries are half-integral, signifying charge fractionalization. Indeed, for N both even and odd, the charge density near left boundary has a spatial profile identical to the charge density near a probe charge $+1/2$.

D. DMRG with a modified Gauss law constraint

Above, we used the standard Gauss law constraint (47), or equivalently (49), for DMRG. The constraint (47) is chosen [31] so that it is satisfied by the ground state $|\mathrm{GS}_0\rangle$ in the "strong coupling limit" ($ga \to +\infty$ with m/g^2a fixed) [44] with vanishing L_n. In terms of the fermion occupation numbers $\chi_n^\dagger\chi_n$, $|\mathrm{GS}_0\rangle$ corresponds to $|010101\ldots\rangle$.

In this subsection we consider a modified version of the Gauss law constraint [32]

$$0 = G_n^{\text{modified}},$$
$$:= L_n - L_{n-1} - \chi_n^\dagger\chi_n + \frac{1}{2} = L_n - L_{n-1} - \frac{Z_n}{2}. \quad (66)$$

Compared with the standard choice (47), we dropped the term $-(-1)^n/2$, which affects the boundary value of the scalar ϕ, as argued in the Appendix of [36].

If the periodic B.C. is chosen, as explained in Appendix B 4 of [33], this modification of the Gauss law constraint is equivalent, via a shift of L_n by $(-1)^n/4$,[17] to a shift of the mass parameter such that the theory with a vanishing shifted mass enjoys a discrete chiral symmetry and

[16] For a similar correspondence in the case of periodic XY models, see Sec. 5.2.2 of [46].

[17] The corresponding manipulation for the open B.C. is (68).

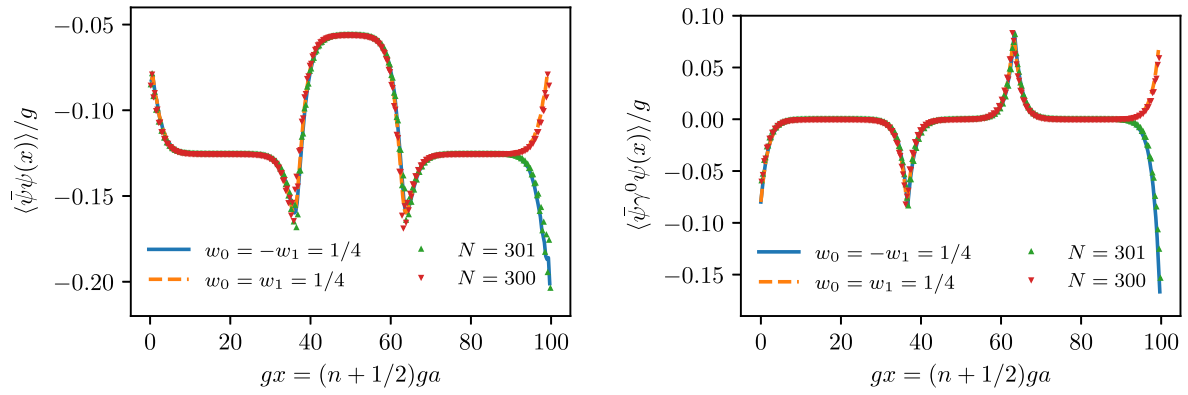

FIG. 5. Plots of (a) the chiral condensate $\langle\bar{\psi}\psi(x)\rangle/g$ and (b) the charge density $\langle\bar{\psi}\gamma^0\psi(x)\rangle/g$. The chiral condensate is computed analytically by (21), and by DMRG as $(4ga)^{-1}(-1)^n\langle Z_n - Z_{n+1}\rangle$. The charge density is computed analytically by (24) and by DMRG as $(4ga)^{-1}\langle Z_n + Z_{n+1}\rangle$. The DMRG computation was done using (56) with $q = 0.3$, $\theta_0 = 0.9$, $ga = 1/3$, $\widehat{\ell} = 80$, $\widehat{\ell}_0 = \lfloor (N - \widehat{\ell} - 1)/2 \rfloor$, $m = 0$, and the values of N indicated in the figure. The analytic results shown as solid and dashed lines are computed for $\Theta(x) = \Theta_{(q,\theta_0-\pi/2)}(x)$ defined in (3) with $\ell = \widehat{\ell}a$ and $\ell_0 = \widehat{\ell}_0 a$.

a faster convergence to the continuum limit. While one has to allow L_n to take noninteger values to satisfy the modified Gauss law (66), one can require the shifted version to take integer values. Solving the modified constraint with the boundary condition $L_{-1} = 0$ and fixing the gauge, we obtain the modified Hamiltonian

$$H_{\text{modified}} = \frac{g^2 a}{2}\sum_{n=0}^{N-2}\left[\frac{1}{2}\sum_{i=0}^{n} Z_i + \frac{\vartheta_n}{2\pi}\right]^2 + \frac{1}{4a}\sum_{n=0}^{N-2}(X_n X_{n+1} + Y_n Y_{n+1}) + \frac{m}{2}\sum_{n=0}^{N-1}(-1)^n Z_n. \tag{67}$$

A direct calculation shows that

$$\left[\frac{1}{2}\sum_{i=0}^{n} Z_i + \frac{\vartheta_n}{2\pi}\right]^2 = \left[\sum_{i=0}^{n}\frac{Z_i + (-1)^i}{2} + \frac{\vartheta_n - \frac{\pi}{2}}{2\pi}\right]^2 - \sum_{i=0}^{N-1}\frac{(-1)^i}{8} Z_i - \frac{(-1)^N}{8} Q + \text{c-number}. \tag{68}$$

Comparing with (51) we see that, within the fixed charge Q sector, the modification (66) of the Gauss law is equivalent to a shift of the mass $m \to m - (g^2 a/8)$ [33] and a shift of the theta angle $\vartheta_n \to \vartheta_n - (\pi/2)$. The latter shift would be further modified if we chose a boundary condition other than $L_{-1} = 0$.

Figure 5 displays the profiles of the chiral condensate $\langle\bar{\psi}\psi(x)\rangle$ and the charge density $\langle\bar{\psi}\gamma^0\psi(x)\rangle$ computed by analytic formulas and DMRG for $m = 0$. Contrary to Fig. 4(b), extrapolation is unnecessary because the modification of the Gauss law, which is partially equivalent to the mass shift of [33], makes the convergence to the continuum limit much faster.

IV. SUMMARY AND DISCUSSION

In this work, we studied three formulations of the Schwinger model: the original fermionic formulation, the bosonized formulation, and the Hamiltonian lattice formulation. We computed analytically physical observables in the ground state using the bosonized formulation and found excellent agreements with the DMRG computations in the lattice formulation. We clarified the correspondence between boundary conditions in different formulations. We studied a nonstandard Gauss law constraint (66) in the lattice formulation, and showed that it is equivalent to the mass shift of [33] and a shift of the theta angle. In accordance with [33], we found that the modification of the Gauss law makes the convergence to the continuum limit faster.

As for future directions, it would be interesting to rederive our analytic results in the path integral formalism, along the line of [28]. It would also be worthwhile to establish the faster convergence more firmly by computing the precise difference between the lattice and continuum Hamiltonians. This should be possible by classifying the potential counterterms to the local observables along the line of [49,50] that deals with the Euclidean path integral. Finally, one should be able to perform DMRG in a similar manner to compute local observables in non-Abelian lattice gauge theories in $1 + 1$ dimensions.

ACKNOWLEDGMENTS

The author thanks M. Honda, E. Itou, Y. Kikuchi, and L. Nagano for collaboration on [36], which motivated this

work. He also thanks Y. Kikuchi for providing useful ITensor codes, based on which he wrote his own. He is grateful to Y. Tanizaki for pointing out an error in [36], whose correction was important in this work. Some of the results in this paper were presented in the workshop "Quantum computing for quantum field theories" held at the Yukawa Institute for Theoretical Physics in January, 2021. This work was supported in part by MEXT-JSPS Grant-in-Aid for Transformative Research Areas (A) "Extreme Universe," No. 21H05190.

APPENDIX A: COMPUTATION OF THE ENERGY BY THE METHOD OF IMAGES

In this appendix we compute the ground state energy of the massless Schwinger model with probe charges, using the effective potential obtained in [42].

By integrating out the matter field and restricting to a static gauge field, the effective Lagrangian, on an infinite spatial line, is found to be

$$\mathcal{L}_{\text{eff}} = \frac{1}{2}(\partial_1 A_0)^2 + \frac{\mu^2}{2}A_0^2 - \rho A_0, \tag{A1}$$

where we introduced the density $\rho(x)$ of external charges. For two charges q_1 and q_2 separated by distance ℓ, $\rho(x) = q_1 g[\delta(x) + q_2\delta(x-\ell)]$, the solution to the Euler-Lagrange equation

$$(-\partial_1^2 + \mu^2)A_0 = \rho \tag{A2}$$

gives the two-body potential [27]

$$V_{q_1,q_2}(\ell) = -\frac{\pi}{2}q_1 q_2 \mu(1 - \mathrm{e}^{-\mu\ell}). \tag{A3}$$

To compute the energy on an interval $[0, L]$, we extend the domain of the charge density $\rho(x)$ from to $(-\infty, \infty)$ as an even periodic function of period $2L$, $\rho(-x) = \rho(x)$, $\rho(x + 2L) = \rho(x)$. We solve (A2) for A_0 using the Green's function $G(x) = \mathrm{e}^{-\mu|x|}/2\mu$ and substitute A_0 to (A2) with the integration range $[0, L]$. The energy given by

$$E = -\int_0^L dx\mathcal{L}_{\text{eff}} = \frac{1}{2}\int_0^L dx\rho(x)A_0(x) \tag{A4}$$

can be evaluated by summing the two-point potential between (1) the probe charges in the interval $[0, L]$, and (2) the probe charges in the interval and image charges.

As an example let us consider the charge distribution $\rho_{\text{pair}}(x) = q\delta(x - \ell_0) - q\delta(x - \ell_0 - \ell)$ with $\ell_0 = (L - \ell)/2$ for $0 < x < L$, shown in Fig. 1. We extend $\rho_{\text{pair}}(x)$ to an even periodic function, which is depicted in Fig. 6. The energy (A4) reproduces (28).

As another example, let us modify the setup in the previous paragraph by adding charges q_L and q_R to the left and right boundaries, respectively. We are interested in the q-dependent part of the energy. To compute it, we sum the two-point potentials between (1) the probe charges in the interval $[0, L]$, (2) the probe charges in the interval and their image charges, and (3) the probe charges in the interval and the boundary charges including their images. The two-point potential between boundary charges is q independent and we drop it. Compared with the previous paragraph, the new contribution is from (3):

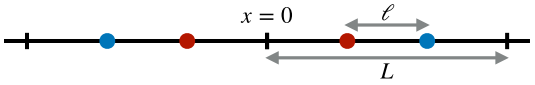

FIG. 6. Charge distribution $\rho_{\text{pair}}(x)$ extended as an even periodic function.

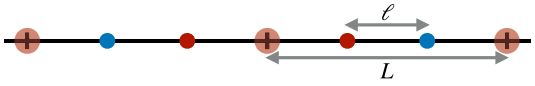

FIG. 7. Charge distribution with boundary charges of the same sign and magnitude added.

$$\Delta E_{\text{pair}} = \frac{\pi\mu}{2}q(q_L - q_R)\frac{\mathrm{e}^{-\frac{\mu}{2}(L-\ell)} - \mathrm{e}^{-\frac{\mu}{2}(L+\ell)}}{1 + \mathrm{e}^{-\mu L}}. \tag{A5}$$

This vanishes if $q_L = q_R$. See Fig. 7.

For $\Theta = \Theta_{\text{pair}}$ in (26) and general w_0 and w_1 in (13), the ground state energy computed from (16) turns out to be

$$(28) + \pi\mu q(w_0 + w_1)\frac{\sinh(\mu\ell/2)}{\cosh(\mu L/2)}. \tag{A6}$$

This is consistent with (A5) by the relations in (65), i.e., $w_0 = q_L/2$ and $w_1 = -q_R/2$. For $w_0 = -w_1 = 1/4$, $\Delta E_{\text{pair}} = 0$. This result appeared and was used in [36]. We checked that the DMRG computation of the ground state energy with large N agrees well (as a function of ℓ) with $E_{\text{pair}} + \Delta E_{\text{pair}}$ for $(q_L, q_R) = (1/2, -1/2)$ if N is even, and for $(q_L, q_R) = (1/2, 1/2)$ if N is odd.

APPENDIX B: EXACT ONE-FORM SYMMETRIES IN LATTICE QCDS IN 1 + 1 DIMENSIONS

In this appendix, we show that the general lattice QCD in the Kogut-Susskind formulation [39] enjoys an exact one-form C_0 symmetry, where C_0 consists of the elements of the center of the gauge group G under which the matter fermions are invariant. The presence of such a center one-form symmetry well known in the continuum limit [51] and is also known for the charge-q lattice Schwinger model [33]. As the discussion for the general lattice QCD is rather abstract, we begin with the charge-q Schwinger model, which can be understood more intuitively.

The charge-q Schwinger model, i.e., the $U(1)$ gauge theory with a single Dirac fermion of charge q, has attracted

attention in recent years. See, e.g., [52,53]. As the defining action we take

$$S = \int d^2x \left[-\frac{1}{4} F_{\mu\nu} F^{\mu\nu} + \frac{g\vartheta}{4\pi} \epsilon_{\mu\nu} F^{\mu\nu} + \mathrm{i}\bar{\psi}\gamma^\mu(\partial_\mu + \mathrm{i}\mathrm{q}gA_\mu)\psi - m\bar{\psi}\psi \right] + \sum_p q_p g \int dt A_t(x_p) + \text{boundary terms}. \tag{B1}$$

Unlike in Sec. II, we define probe charges using couplings separate from the theta angle. We also take q_p to be integers so that the corresponding Wilson lines are genuine line operators rather than boundaries of topological surface operators. The bosonized Lagrangian is

$$\mathcal{L} = -\frac{1}{4} F_{\mu\nu} F^{\mu\nu} + \frac{g}{4\pi} \vartheta \epsilon^{\mu\nu} F_{\mu\nu} + \frac{\mathrm{q}g}{\sqrt{\pi}} \epsilon^{\mu\nu} A_\mu \partial_\nu \phi + \frac{1}{2} \partial_\mu \phi \partial^\mu \phi + mg \frac{\mathrm{e}^\gamma}{2\pi^{3/2}} \cos(2\sqrt{\pi}\phi) + \sum_p q_p g \delta(x - x_p) A_t(x). \tag{B2}$$

The Gauss law constraint reads

$$\partial_1 \left(F_{01} - \frac{g}{2\pi}(\vartheta + 2\mathrm{q}\sqrt{\pi}\phi) \right) = \sum_p q_p g \delta(x - x_p). \tag{B3}$$

The theory possesses a $\mathbb{Z}_\mathrm{q}$ one-form symmetry, whose generator can be expressed in the bosonized form [52,53]

$$V_\mathrm{q} \coloneqq \exp\left[\frac{2\pi\mathrm{i}}{\mathrm{q}g} \left(F_{01} - \frac{g}{2\pi}\vartheta - \frac{\mathrm{q}g}{\sqrt{\pi}}\phi \right) \right], = \exp\left(\sum_p \frac{2\pi\mathrm{i}}{\mathrm{q}} q_p H_\mathrm{step}(x - x_p) \right).$$

This is piecewise constant as a topological operator should be, and labels the distinct decomposed sectors of the theory called "universes" [54–58].

The corresponding Hamiltonian of the lattice theory in the presence of probe charges is

$$H_\mathrm{lattice} = J \sum_{n=0}^{N-2} \left(L_n + \frac{\vartheta}{2\pi} \right)^2 - \mathrm{i}w \sum_{n=0}^{N-2} \left[\chi_n^\dagger (U_n)^\mathrm{q} \chi_{n+1} - \chi_{n+1}^\dagger (U_n^\dagger)^\mathrm{q} \chi_n \right] + m \sum_{n=0}^{N-1} (-1)^n \chi_n^\dagger \chi_n.$$

Again, we work in a formulation slightly different from Sec. III and [52] and implement the effects of probe charges by adding the corresponding terms in the Gauss law constraint

$$L_n - L_{n-1} + \mathrm{q}\left[-\chi_n^\dagger \chi_n + \frac{1 - (-1)^n}{2} \right] = \sum_p q_p \delta_{n n_p}. \tag{B4}$$

In terms of spin variables we have

$$L_n - L_{n-1} - \mathrm{q}\frac{Z_n + (-1)^n}{2} = \sum_p q_p \delta_{n n_p}. \tag{B5}$$

The lattice generator of the $\mathbb{Z}_\mathrm{q}$ one-form symmetry, corresponding to (B4), is [33]

$$V_\mathrm{q} = \exp\left[\frac{2\pi\mathrm{i}}{\mathrm{q}} \left(L_n - \frac{\mathrm{q}}{2} \sum_{i=0}^{n} (Z_i + (-1)^i) \right) \right] = \exp\left(\frac{2\pi\mathrm{i}}{\mathrm{q}} L_n \right), \tag{B6}$$

where we used the correspondences (57) and (58) and the fact that $Z_i + (-1)^i$ vanishes mod 2. As in the continuum case, the Gauss law (B5) implies that V_q acting on a physical state is almost constant as a function of the position but gets multiplied by a phase as one crosses probe charges q_p (temporal Wilson lines) at $n = n_p$. This means, by the Wick rotation and the exchange of space and time, that V_q obeys the expected commutation relations with the Wilson lines.[18]

We now turn to an arbitrary Hamiltonian lattice gauge theory with a general gauge group G and a fermion in representation ρ [39]. For G we only require that it is compact: it can be non-Abelian, discrete, a product, a quotient, or something more complicated. The Lie algebra $\mathfrak{g}$ of G decomposes into simple Lie algebras

$$\mathfrak{g} = \bigoplus_b \mathfrak{g}_b. \tag{B7}$$

The maximal torus T of G has the Lie algebra $\mathfrak{t} = \oplus_b \mathfrak{t}_b$, where $\mathfrak{g}$ and $\mathfrak{g}_b$ are the Cartan subalgebras of $\mathfrak{g}$ and $\mathfrak{g}_b$, respectively. The center C of G has the Lie algebra $\mathfrak{c} = \oplus_i \mathfrak{c}_i$, where $\mathfrak{c}_i \simeq \mathbb{R}$ is the Lie algebra of the "$U(1)$ factor" labeled by i. In general ρ is reducible:

$$\rho = \bigoplus_f \rho_f, \tag{B8}$$

where ρ_f is an irreducible representation of G. Again we consider a one-dimensional lattice with sites labeled by $n = 0, 1, \ldots N-1$. The Hilbert space of the theory is the tensor product of the local Hilbert spaces associated with sites $n \in \{0, \ldots, N-1\}$ and links $n \in \{0, \ldots, N-2\}$.

[18] In [48] it was demonstrated that the complexified chiral condensate $\langle \bar{\psi} e^{\mathrm{i}\gamma_5} \psi \rangle$ flows in the IR to the topological operator V_q.

On each site n, we have a fermion Fock space, possibly tensored with the representation space for a probe charge. The fermionic Fock space is generated by the fermion $\chi_n = (\chi_n^f)_f$ in representation $\rho = \oplus_f \rho_f$ and its Hermitian conjugate. In addition, if we place a probe charge in representation R_p on site n_p, we tensor the Fock space with the representation space V_p of R_p. On each link n we have the space of square-integrable functions on G. The total Hilbert space is thus of the form

$$\mathcal{H}_{\text{total}} = \mathcal{H}_{\text{fermion}} \otimes \mathcal{H}_{\text{gauge}} \otimes \mathcal{H}_{\text{probe}}. \tag{B9}$$

The Hamiltonian takes the form[19]

$$\begin{aligned} H_{\text{lattice}} = &\sum_b J_b \sum_{n=0}^{N-2} \mathrm{tr}\left(L_n^b + \frac{\delta_{bi}\vartheta_i}{2\pi}\right)^2 \\ &- \mathrm{i}w \sum_{n=0}^{N-2} (\chi_n^\dagger \rho(g_n)\chi_{n+1} - \chi_{n+1}^\dagger \rho(g_n)^\dagger \chi_n) \\ &+ \sum_f m_f \sum_{n=0}^{N-1} (-1)^n (\chi_n^f)^\dagger \chi_n^f, \end{aligned} \tag{B10}$$

where $w = 1/2a$, $J_\alpha = g_b^2 a/2$, g_b is the coupling constant for $\mathfrak{g}_b$, ϑ_i is the theta angle for $\mathfrak{c}_i$, and m_f is the mass for the fermion labeled by f. The trace tr is taken in a faithful irreducible representation of G, in which g_n is represented by a unitary matrix U_n. The $\mathfrak{g}_b$ part of the "left" canonical momentum $L_n = \oplus_b L_n^b$ conjugate to $g_n \in G$ can be expanded as $L_n = L_{\alpha n} T^\alpha$ and obeys (in our sign convention) the canonical commutation relation

$$[g_m, L_{\alpha n}] = \delta_{mn} T_\alpha g_m, \tag{B11}$$

where $T_\alpha = \kappa_{\alpha\beta} T^\beta$, the matrix $\kappa_{\alpha\beta}$ is the inverse of $\kappa^{\alpha\beta} = \mathrm{tr}(T^\alpha T^\beta)$, which is a Killing form of $\mathfrak{g}$. Let us define $R_n := g_n^{-1} L_n g_n$. Then one can show that $R_{\alpha n}$ defined by $R_n = R_{\alpha n} T^\alpha$ satisfies the commutation relation

$$[g_m, R_{\alpha n}] = \delta_{mn} g_m T_\alpha. \tag{B12}$$

The group $\mathcal{G}$ of gauge transformations is the product of copies of G, each associated with a site n. The gauge transformation $h_n \in G$ on site n acts as

$$\begin{aligned} &\chi_n \to \rho(h_n)\chi_n, \qquad g_n \to h_n g_n h_{n+1}^{-1}, \\ &L_n \to h_n L_n h_n^{-1}, \qquad R_n \to h_{n+1} R_n h_{n+1}^{-1}, \end{aligned} \tag{B13}$$

and leaves the Hamiltonian invariant and the canonical commutation relations invariant. For the continuous part of the gauge group, the Gauss law constraints are

$$L_n^\alpha - R_{n-1}^\alpha - \chi_n^\dagger T^\alpha \chi_n + \frac{1-(-1)^n}{2}\mathrm{tr}(T^\alpha) = \sum_p \delta_{nn_p} T_p^\alpha,$$

where T_p^α are the generators in the representations R_p for probe charges. It is possible to consider, as in (66), the modified version of the Gauss law constraint where the term containing $(-1)^n$ is dropped.

If the gauge group G contains as a factor the cyclic group $\mathbb{Z}_d = \{\mathrm{e}^{(2\pi\mathrm{i}/d)j} | j = 0, 1, \ldots, d-1\}$, on each link there exist operators Z_n and X_n such that $Z_m X_n = \exp[(2\pi\mathrm{i}/d)\delta_{mn}] X_n Z_m$, $Z_n^d = X_n^d = 1$. The Gauss law constraint takes the group form

$$\begin{aligned} &X_n X_{n-1}^{-1} \exp\left[\frac{2\pi\mathrm{i}}{d}\left(-\chi_n^\dagger D \chi_n + \frac{1-(-1)^n}{2}\mathrm{tr}D\right)\right] \\ &= \exp\left[\frac{2\pi\mathrm{i}}{d}\sum_s q_s \delta_{nn_s}\right], \end{aligned} \tag{B14}$$

where D is a diagonal matrix of $\mathbb{Z}_d$ charges (integers modulo d) for the fermion, and q_s are the $\mathbb{Z}_d$ charges of the probes at $n = n_s$.

For a general gauge group (including non-Abelian discrete groups such as the dihedral group D_4) instead of imposing the Gauss law constraint in terms of operators, we can simply project the total Hilbert space $\mathcal{H}_{\text{total}}$ onto the physical Hilbert space $\mathcal{H}_{\text{phys}}$, which is the subspace of $\mathcal{H}_{\text{total}}$ invariant under the group $\mathcal{G}$ of gauge transformations [59].

To study one-form symmetries, let C_0 consist of the elements of the center C (of the gauge group G) under which the fermion χ_n is invariant. Since C_0 is Abelian and compact, it is of the form $C_0 = U(1)^M \times \Gamma$, where Γ is a product of cyclic groups. On each site n and for $c \in C_0$, let us consider the operator $\mathrm{Gauge}_n(c)$ implementing the gauge transformation corresponding to c^{-1}.[20] It is of the form

$$\mathrm{Gauge}_n(c) = \mathrm{Left}_n(c^{-1})\mathrm{Right}_{n-1}(c)\mathrm{R}_p(c^{-1})^{\delta_{nn_p}},$$

where $\mathrm{Left}_n(h)$ [respectively, $\mathrm{Right}_n(h)$] is the operator corresponding to the left (respectively, right) action of h on the copy of G on link n. The appearance of $\mathrm{Left}_n(c^{-1})$ and $\mathrm{Right}_{n-1}(c)$ can be understood from (B13). The operator $\mathrm{R}_p(c^{-1})^{\delta_{nn_p}}$ represents the action of c^{-1} on the representation space V_p for the probe p. Because c is in the center, in fact we have $\mathrm{Left}_n(c^{-1}) = \mathrm{Right}_n(c^{-1}) =: V_n(c)$.

[19]We do not include a kinetic term for the discrete part of the gauge group. Thus if the whole gauge group is discrete and there is no matter, the gauge theory is topological.

[20]Here we use c^{-1} instead of c to be consistent with earlier definitions of one-form symmetry generators.

On the physical Hilbert space $\mathcal{H}_{\text{phys}}$, which is invariant under gauge transformations, we have the equality $V_n(c)V_{n-1}(c)^{-1}\mathrm{R}_p(c^{-1})^{\delta_{nn_p}} = 1$ or equivalently

$$V_n(c) = V_{n-1}(c)\mathrm{R}_p(c)^{\delta_{nn_p}}. \tag{B15}$$

Since c is in the center and R_p is an irreducible representation, $\mathrm{R}_p(c) = \exp[\mathrm{i}\alpha_{R_p}(c)]$ is in fact a c-number corresponding to the charge under C_0. Equation (B15) establishes that $V_n(c)$ is the generator of the one-form symmetry for C_0. It is constant between probe charges, and obeys the expected commutation relation between Wilson line operators $W_{\mathrm{R}} = \mathrm{Tr}_{\mathrm{R}} P \exp(\mathrm{i}\oint A)$:

$$W_{\mathrm{R}} V(c) = \mathrm{e}^{\mathrm{i}\alpha_R(c)} V(c) W_{\mathrm{R}}, \tag{B16}$$

which we rewrote as an operator relation via a Wick rotation and a rotation in the Euclidean spacetime.

[1] J. S. Schwinger, Gauge invariance and mass. 2., Phys. Rev. **128**, 2425 (1962).
[2] T. Byrnes, P. Sriganesh, R. J. Bursill, and C. J. Hamer, Density matrix renormalization group approach to the massive Schwinger model, Phys. Rev. D **66**, 013002 (2002).
[3] M. C. Bañuls, K. Cichy, K. Jansen, and J. I. Cirac, The mass spectrum of the Schwinger model with matrix product states, J. High Energy Phys. 11 (2013) 158.
[4] M. C. Bañuls, K. Cichy, J. I. Cirac, K. Jansen, and H. Saito, Matrix product states for lattice field theories, Proc. Sci. LATTICE2013 (**2014**) 332 [arXiv:1310.4118].
[5] E. Rico, T. Pichler, M. Dalmonte, P. Zoller, and S. Montangero, Tensor Networks for Lattice Gauge Theories and Atomic Quantum Simulation, Phys. Rev. Lett. **112**, 201601 (2014).
[6] B. Buyens, J. Haegeman, K. Van Acoleyen, H. Verschelde, and F. Verstraete, Matrix Product States for Gauge Field Theories, Phys. Rev. Lett. **113**, 091601 (2014).
[7] M. C. Bañuls, K. Cichy, J. I. Cirac, K. Jansen, and H. Saito, Thermal evolution of the Schwinger model with matrix product operators, Phys. Rev. D **92**, 034519 (2015).
[8] M. C. Bañuls, K. Cichy, K. Jansen, and H. Saito, Chiral condensate in the Schwinger model with matrix product operators, Phys. Rev. D **93**, 094512 (2016).
[9] L. Funcke, K. Jansen, and S. Kühn, Topological vacuum structure of the Schwinger model with matrix product states, Phys. Rev. D **101**, 054507 (2020).
[10] T. V. Zache, M. Van Damme, J. C. Halimeh, P. Hauke, and D. Banerjee, Toward the continuum limit of a $(1+1)$D quantum link Schwinger model, Phys. Rev. D **106**, L091502 (2022).
[11] J. C. Halimeh, M. Van Damme, T. V. Zache, D. Banerjee, and P. Hauke, Achieving the quantum field theory limit in far-from-equilibrium quantum link models, Quantum **6**, 878 (2022).
[12] E. A. Martinez *et al.*, Real-time dynamics of lattice gauge theories with a few-qubit quantum computer, Nature (London) **534**, 516 (2016).
[13] C. Muschik, M. Heyl, E. Martinez, T. Monz, P. Schindler, B. Vogell, M. Dalmonte, P. Hauke, R. Blatt, and P. Zoller, U(1) Wilson lattice gauge theories in digital quantum simulators, New J. Phys. **19**, 103020 (2017).
[14] H. Bernien *et al.*, Probing many-body dynamics on a 51-atom quantum simulator, Nature (London) **551**, 579 (2017).
[15] F. M. Surace, P. P. Mazza, G. Giudici, A. Lerose, A. Gambassi, and M. Dalmonte, Lattice Gauge Theories and String Dynamics in Rydberg Atom Quantum Simulators, Phys. Rev. X **10**, 021041 (2020).
[16] N. Klco, E. F. Dumitrescu, A. J. McCaskey, T. D. Morris, R. C. Pooser, M. Sanz, E. Solano, P. Lougovski, and M. J. Savage, Quantum-classical computation of Schwinger model dynamics using quantum computers, Phys. Rev. A **98**, 032331 (2018).
[17] C. Kokail *et al.*, Self-verifying variational quantum simulation of lattice models, Nature (London) **569**, 355 (2019).
[18] G. Magnifico, M. Dalmonte, P. Facchi, S. Pascazio, F. V. Pepe, and E. Ercolessi, Real time dynamics and confinement in the $\mathbb{Z}_n$ Schwinger-Weyl lattice model for $1+1$ QED, Quantum **4**, 281 (2020).
[19] B. Yang, H. Sun, R. Ott, H.-Y. Wang, T. V. Zache, J. C. Halimeh, Z.-S. Yuan, P. Hauke, and J.-W. Pan, Observation of gauge invariance in a 71-site Bose–Hubbard quantum simulator, Nature (London) **587**, 392 (2020).
[20] B. Chakraborty, M. Honda, T. Izubuchi, Y. Kikuchi, and A. Tomiya, Classically emulated digital quantum simulation of the Schwinger model with a topological term via adiabatic state preparation, Phys. Rev. D **105**, 094503 (2022).
[21] D. E. Kharzeev and Y. Kikuchi, Real-time chiral dynamics from a digital quantum simulation, Phys. Rev. Res. **2**, 023342 (2020).
[22] A. Yamamoto, Quantum variational approach to lattice gauge theory at nonzero density, Phys. Rev. D **104**, 014506 (2021).
[23] W. A. de Jong, K. Lee, J. Mulligan, M. Płoskoń, F. Ringer, and X. Yao, Quantum simulation of nonequilibrium dynamics and thermalization in the Schwinger model, Phys. Rev. D **106**, 054508 (2022).
[24] Z.-Y. Zhou, G.-X. Su, J. C. Halimeh, R. Ott, H. Sun, P. Hauke, B. Yang, Z.-S. Yuan, J. Berges, and J.-W. Pan, Thermalization dynamics of a gauge theory on a quantum simulator, Science **377**, 311 (2022).
[25] J. Mildenberger, W. Mruczkiewicz, J. C. Halimeh, Z. Jiang, and P. Hauke, Probing confinement in a $\mathbb{Z}_2$ lattice gauge theory on a quantum computer, arXiv:2203.08905.

[26] J. Preskill, Quantum computing in the NISQ era and beyond, Quantum **2**, 79 (2018).
[27] S. Iso and H. Murayama, Hamiltonian formulation of the Schwinger model: Nonconfinement and screening of the charge, Prog. Theor. Phys. **84**, 142 (1990).
[28] I. Sachs and A. Wipf, Finite temperature Schwinger model, Helv. Phys. Acta **65**, 652 (1992), https://www.e-periodica.ch/digbib/view?pid=hpa-001%3A1992%3A65%3A%3A768#654.
[29] S. Durr, Aspects of quasi-phase-structure of the Schwinger model on a cylinder with broken chiral symmetry, Ann. Phys. (N.Y.) **273**, 1 (1999).
[30] Y.-C. Kao and Y.-W. Lee, Schwinger model on a half line, Phys. Rev. D **65**, 067701 (2002).
[31] C. J. Hamer, W.-h. Zheng, and J. Oitmaa, Series expansions for the massive Schwinger model in Hamiltonian lattice theory, Phys. Rev. D **56**, 55 (1997).
[32] F. Berruto, G. Grignani, G. Semenoff, and P. Sodano, Chiral symmetry breaking on the lattice: A study of the strongly coupled lattice Schwinger model, Phys. Rev. D **57**, 5070 (1998).
[33] R. Dempsey, I. R. Klebanov, S. S. Pufu, and B. Zan, Discrete chiral symmetry and mass shift in the lattice Hamiltonian approach to the Schwinger model, Phys. Rev. Res. **4**, 043133 (2022).
[34] S. R. Coleman, R. Jackiw, and L. Susskind, Charge shielding and quark confinement in the massive Schwinger model, Ann. Phys. (N.Y.) **93**, 267 (1975).
[35] S. R. Coleman, More about the massive Schwinger model, Ann. Phys. (N.Y.) **101**, 239 (1976).
[36] M. Honda, E. Itou, Y. Kikuchi, L. Nagano, and T. Okuda, Classically emulated digital quantum simulation for screening and confinement in the Schwinger model with a topological term, Phys. Rev. D **105**, 014504 (2022).
[37] S. R. White, Density Matrix Formulation for Quantum Renormalization Groups, Phys. Rev. Lett. **69**, 2863 (1992).
[38] S. R. White, Density-matrix algorithms for quantum renormalization groups, Phys. Rev. B **48**, 10345 (1993).
[39] J. B. Kogut and L. Susskind, Hamiltonian formulation of Wilson's lattice gauge theories, Phys. Rev. D **11**, 395 (1975).
[40] J. Polchinski, *String Theory. Vol. 2: Superstring Theory and Beyond*, Cambridge Monographs on Mathematical Physics (Cambridge University Press, Cambridge, Enlgand, 2007).
[41] A. Casher, J. B. Kogut, and L. Susskind, Vacuum polarization and the absence of free quarks, Phys. Rev. D **10**, 732 (1974).
[42] D. J. Gross, I. R. Klebanov, A. V. Matytsin, and A. V. Smilga, Screening versus confinement in (1 + 1)-dimensions, Nucl. Phys. **B461**, 109 (1996).
[43] S. R. Coleman, The quantum Sine-Gordon equation as the massive thirring model, Phys. Rev. D **11**, 2088 (1975).
[44] T. Banks, L. Susskind, and J. B. Kogut, Strong coupling calculations of lattice gauge theories: (1 + 1)-dimensional exercises, Phys. Rev. D **13**, 1043 (1976).
[45] P. Jordan and E. P. Wigner, About the Pauli exclusion principle, Z. Phys. **47**, 631 (1928).
[46] E. Fradkin, *Field Theories of Condensed Matter Physics* (Cambridge University Press, Cambridge, England, 2013), 2nd ed.
[47] M. Fishman, S. R. White, and E. M. Stoudenmire, The ITensor software library for tensor network calculations, SciPost Phys. Codebases 4 (2022).
[48] M. Honda, E. Itou, and Y. Tanizaki, DMRG study of the higher-charge Schwinger model and its 't Hooft anomaly, J. High Energy Phys. 11 (2022) 141.
[49] M. Luscher, S. Sint, R. Sommer, and P. Weisz, Chiral symmetry and O(a) improvement in lattice QCD, Nucl. Phys. **B478**, 365 (1996).
[50] M. Luscher, Advanced lattice QCD, in *Les Houches Summer School in Theoretical Physics, Session 68: Probing the Standard Model of Particle Interactions* (1998), pp. 229–280, arXiv:hep-lat/9802029.
[51] D. Gaiotto, A. Kapustin, N. Seiberg, and B. Willett, Generalized global symmetries, J. High Energy Phys. 02 (2014) 172.
[52] M. Honda, E. Itou, Y. Kikuchi, and Y. Tanizaki, Negative string tension of a higher-charge Schwinger model via digital quantum simulation, Prog. Theor. Exp. Phys. **2022**, 033B01 (2022).
[53] A. Cherman, T. Jacobson, and M. Neuzil, Universal deformations, SciPost Phys. **12**, 116 (2022).
[54] T. Pantev and E. Sharpe, Notes on gauging noneffective group actions, arXiv:hep-th/0502027.
[55] T. Pantev and E. Sharpe, String compactifications on Calabi-Yau stacks, Nucl. Phys. **B733**, 233 (2006).
[56] T. Pantev and E. Sharpe, GLSM's for gerbes (and other toric stacks), Adv. Theor. Math. Phys. **10**, 77 (2006).
[57] S. Hellerman and E. Sharpe, Sums over topological sectors and quantization of Fayet-Iliopoulos parameters, Adv. Theor. Math. Phys. **15**, 1141 (2011).
[58] Y. Tanizaki and M. Ünsal, Modified instanton sum in QCD and higher-groups, J. High Energy Phys. 03 (2019) 123.
[59] H. Lamm, S. Lawrence, and Y. Yamauchi (NuQS Collaboration), General methods for digital quantum simulation of gauge theories, Phys. Rev. D **100**, 034518 (2019).